CIMAC CONGRESS 25
ZURICH, MAY 19 – 23, 2025

2025 | 523

Usage of 1-D system simulation for the development of a maritime PEM-Fuel cell system

Electrification and Fuel Cells Development

Stephan Karmann, Freudenberg

Stephan Karmann, Freudenberg e-power Systems
Jacub Pazdera, Freudenberg Fuell Cells and e-Power Systems
Karl Runge, Freudenberg Fuell Cells and e-Power Systems

ABSTRACT

As two thirds of global freight transport is handled by shipping and accounts for 2% of global CO2 emissions, there is great potential for a reduction. With the upcoming commitment of the IMO to have a carbon neutral shipping until 2050 the development of maritime propulsion systems is under high pressure to reach this ambitious goal.

An important step that is currently the focus of research is the usage of renewable and sustainable fuels for maritime propulsion systems. Amongst them are methanol, ammonia and hydrogen which have proven their potential to be sustainably produced by electrolysis using renewable energies and carbon capturing. Due to limited storage capacity on board, hydrogen with its comparably low energy density seems not to be a suitable alternative at the moment. Hence, methanol and ammonia stored in liquid form on the ship are a more promising approach.

Therefore, Freudenberg e-Power systems is developing a compact maritime fuel cell system based on steam reformation of methanol to hydrogen coupled with low temperature polymer-electrolyte fuel cells for transferring the chemically bound energy to electricity. With this system a complete electrified propulsion and energy distribution system on board can be realized without any further generator losses. The low temperature polymer-electrolyte fuel cell shows high efficiencies thus provides an alternative to internal combustion engines. Further drawbacks as lube oil combustion, increased backfiring potential if hydrogen is used, noise vibration and harshness and NOx-emissions due to high combustion temperatures can be overcome.

The maritime fuel cell system consists of the hydrogen generation module conducting the steam reformation to supply reformate gas to the fuel cell module containing six fuel cells with a power output of 110kW each. For the development and validation, a detailed 1D-System model is being implemented. This multi-physical model is being used to virtually verify the system’s functionality with its chemical and electro-chemical process, components and operating strategy.

First comparisons of testing rig data of the fuel cell and the simulation proved the methodology to improve the design and performance of the systems developed. Further a comprehensive effort has been made to gain high accuracy for the hydrogen supply units’ main components conducting the reformation and purification process. For this reason, preliminary experimental tests to determine the reaction kinetics have been carried out and are used to calibrate the simulation. With this in-depth simulation of the maritime fuel cell module the quality of the first physical prototype can be enhanced to assure a more efficient development.

1 INTRODUCTION

Environmental concerns due to greenhouse gas (GHG) emissions and safety of public health due to particle matters induce an urgent need for sustainable energy solutions across all transportation modes worldwide. Marine energy supply systems, responsible for about 3% of global GHG emissions, are under significant pressure to adopt carbon-neutral alternatives. [1]
Current regulations, such as the EU Emission Trading System (ETS) of 2024 and the upcoming FuelEU Maritime directive for 2025, establish a progressive framework for decarbonizing maritime propulsion systems. Within this regulatory context, the International Maritime Organization (IMO) has set a comprehensive agenda to achieve net-zero GHG emissions by 2050, focusing on:
Technological measures: Emphasizing alternative, less GHG-intensive maritime fuels and enhanced propulsion system efficiency.
Economic measures: Implementing pricing mechanisms and trading schemes for GHG emissions to drive the development of GHG-saving technologies.
The technological measures include exploring hydrogen (H_2), methanol (CH_3OH), and ammonia (NH_3) as future green fuels with neutral carbon footprint (cf. [2]). Additionally, onboard battery storage systems coupled with fully electric or hybrid propulsion systems are part of the strategies being explored to decarbonize maritime propulsion (cf. [3]).

Figure 1 shows the energy density of alternative fuels and battery storage systems relative to conventional fossil fuels used in the maritime industry.

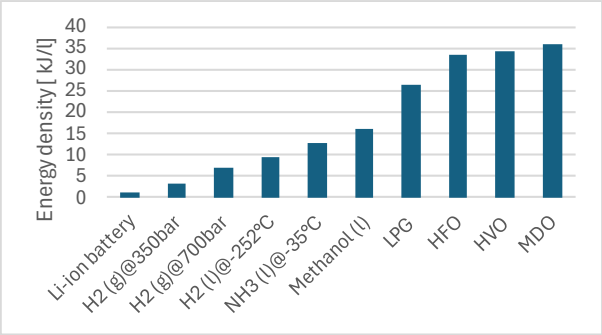

Figure 1 Energy density of alternative and conventional maritime energy storage systems (cf. [4])

The data reveals that alternative fuels require 2 to 4 times more storage volume than greenhouse gas-intensive marine diesel oil (MDO). Despite its limitations methanol offers significant environmental and practical advantages as an alternative fuel. When burned in internal combustion engines (ICEs), grey methanol reduces CO_2 emissions by 7.8% compared to MDO per kilogram. (cf. [4–6]). Additionally, methanol combustion results in a 60% reduction in nitrogen oxides (NOx) emissions and a 95% reduction in sulfur oxides (SOx) and particulate matter (PM) compared to MDO. Moreover, methanol can be produced from renewable sources like biomass or surplus sustainable electricity and carbon capturing, which helps lower overall GHG emissions by over 90% compared to production from conventional fossil fuels like natural gas (NG) (cf. [7]).

Using ammonia as a fuel in an ICE results in no CO_2 emissions, as ammonia (NH3) does not contain carbon (cf. [8]). However, ammonia requires approximately 2.3 times the amount of fuel to produce the same amount of energy as MDO comparable to methanol with a factor of around 2.1 (cf. [9]). Due to the high nitrogen content in ammonia, the combustion process leads to increased NO_x emissions, which are exacerbated by the high temperatures necessary for efficient combustion. Compared to conventional fossil fuels ammonia offers a low laminar burning velocity resulting in even lower combustion efficiency. NO_x emissions can be mitigated through advanced exhaust gas aftertreatment systems or by employing advanced and more complex combustion processes (RCCI, HCCI). [10–12] Compared to methanol, ammonia also poses a higher safety risk despite both being toxic. Ammonia in particular is more challenging to handle due to its corrosive nature. [13, 14])

The utilization of hydrogen as a fuel in ICEs is comparable to that of ammonia. Hydrogen combustion does not produce CO_2, thereby eliminating a major greenhouse gas. However, due to hydrogen's high laminar burning velocity, the combustion process results in elevated temperatures, leading to the formation of NOx emissions, thus necessitating further internal and external measures for reduction. Additionally, hydrogen combustion can exhibit abnormal combustion phenomena like knock, pre-ignition, and backfire arising for example from lube oil combustion (cf. [15, 16]. Compared to ammonia, methanol and MDO, hydrogen's energy density is significantly lower, by up to a factor of five, necessitating significantly more bunkering space. Additionally, hydrogen storage requires additional energy: 1.7-6.4 kWh/kg for compressed H_2 and 7-13 kWh/kg for liquefied H_2, whereas methanol and MDO can be stored without any need for additional energy (cf. [17]).

Batteries provide the lowest energy density compared to conventional fuels, making them advantageous for hybrid system applications. Their

integration enhances operational flexibility, leading to improved fuel efficiency, reduced emissions, and decreased noise levels. This is particularly beneficial when they enable a ship to operate for limited periods without relying on the ICE, especially for maneuvers in the harbor or in emission-controlled areas (ECA) (cf. [18]).

Because of the drawbacks of state-of-the-art maritime energy supply using ICEs with fossil fuels or even sustainable fuels, whose SO_x or NO_x emissions necessitate complex aftertreatment systems, alternative energy conversion methods are becoming increasingly attractive for maritime power supply on board. One of the most promising technologies are fuel cells (cf. [19, 20]). Fuel cells offer reduced emissions, higher thermodynamic efficiency compared to ICEs, quiet operation due to the lack of rotating components and pulsed power output, high scalability, and flexibility in power output, application, installation and design. Several studies [21–23] highlight proton exchange membrane (PEMFC), solid oxide (SOFC) and molten carbonate fuel cells (MCFC) as promising for maritime power supply applications. Table 1 compares these three fuel cell technologies regarding operating temperature, lifetime, usable fuel, power density and efficiency.

Table 1 Comparison of fuel cell types (cf. [24, 25])

Criteria	**PEMFC**	**SOFC**	**MCFC**
Op. temperature [°C]	60-100	500-1000	600-700
Lifetime rating	3	1	1
Fuel	H_2	H_2, NG	various
Power density [W/cm²]	0.5-2.5	0.2-1.5	0.1-0.3
Efficiency [%]	50-60	50-65	45-55

Van Biert [26] highlights that SOFCs are ideal for maritime applications due to their fuel flexibility, long lifetime, and still moderate power density. On the other hand, PEMFCs are particularly suitable for smaller vessels and power supply applications because of their superior start-up behavior and high-power density. Moreover, PEMFCs are more mature and continue to be optimized and researched, being already in use in automotive (cf. [27, 28]) and maritime applications (cf. [29, 30]). For the latter, a regulatory framework is being developed already (cf. [31, 32]). Nevertheless, the widespread adoption of this future maritime power supply faces several challenges, including technical issues related to the development and the need for advanced materials that impact the fuel cell's lifetime and efficiency, as well as safety concerns regarding onboard hydrogen supply, and economic issues related to the necessary hydrogen infrastructure and high initial costs of PEMFCs. However, these challenges are being gradually addressed by ongoing research (e.g. [33]) and optimizations.

To support this effort, Freudenberg Fuel Cell e-Power Systems GmbH is developing a compact maritime fuel cell system designed to provide 500 kW of electrical net power per unit onboard (cp. [34]). To overcome the disadvantage of hydrogen storage and distribution onboard and limited operation range, Freudenberg's approach is to produce the necessary hydrogen for the low-temperature PEMFC directly out of available fuels, such as the promising renewable fuel methanol on board. This allows for a single fuel storage system, for a hybrid setup using e.g. methanol ICEs and the maritime fuel cell system in varying numbers to match the vessel's power demand as well as resolving the disadvantages that arise from storing pure hydrogen. Therefore, the maritime fuel cell system includes a hydrogen generation module that conducts methanol steam reformation to supply hydrogen-rich reformate gas to the fuel cell module.

This paper provides an overview of how 1D-system simulation supports the development and optimization of Freudenberg's maritime fuel cell systems. Gamma Technologies' GT-Suite is being used to gain deep insights into the steady-state and dynamic behavior of individual components and the complete system. This includes functional, thermal, electrochemical, and flow analysis. To develop a reliable model, preliminary tests and supplier data have been incorporated. Thus, 1D system simulation plays a crucial role in developing maritime fuel cell systems.

2 SYSTEM DESCRIPTION

Freudenberg's approach for a sustainable maritime fuel cell system uses hydrogen-rich reformate generated from steam reforming to run a low-temperature (LT) PEMFC. This approach is unique considering the current maritime research landscape summarized in [35], where most PEMFCs fueled with compressed or liquefied hydrogen operate vessels near the shore for short distances.

Despite the current focus on pure hydrogen storage systems, Russo et al. [36] proposed an autothermal oxidative methanol steam reformation process combined with a high-temperature (HT) PEMFC. This approach leverages the higher CO tolerance of the HT-PEMFC and integrates in situ hydrogen production, demonstrating the feasibility of the process and heat integration. Similarly, Lee et al. [37] conducted a comparative simulation study, proposing a detailed specification for a methanol steam reformation process similar to Freudenberg's concept. However, their simulative

study already included a carbon capture unit and utilized an HT PEMFC instead of a LT one.

2.1 Setup of the system

Freudenberg's maritime fuel cell system is based on a heavy-duty LT PEMFC platform, suitable for both on-road and off-road mobile applications with pure hydrogen, as well as maritime applications with reformat gas. To be able to capitalize on the LT PEMFC's advantages of compactness, power density, quick start-up time, and high efficiency, the purity of the reformat becomes a key enabler for the complete system's functionality and efficiency. Current PEMFC catalysts are also prone to the impurities of the gas especially for CO. CO can adsorb on the platinum present in the PEMFC's catalyst and block the active sites leading to a reduced performance. This at least is reversible by oxidizing the CO to CO_2 on the catalyst (cf. [23]) by adding O_2 or using sophisticated platinum ruthenium catalysts (cf. [38]) to promote the oxidation of CO. Nevertheless, the fuel reforming process has to be designed to guarantee a sufficient gas quality with <20 ppm (cf. [34]) CO at all operating points of the system.

The maritime fuel cell system can be separated into two subsystems – the hydrogen supply module (H2MO) and the fuel cell module (FCMO) (cf. Figure 2) each conducting a part of the overall energy conversion. The H2MO system encompasses all balance of plant components involved in the fuel reforming process. Water and methanol are supplied by the ship's infrastructure and vaporized within the system utilizing exhaust heat. This vaporized mixture is then introduced into the tubular reformer with a precise steam-to-carbon (SC) ratio. The endothermic reaction's required thermal energy is produced in a burner. This burner operates by leveraging the hydrogen surplus from the over-stoichiometric operation of the LT PEMFC to generate the necessary heat through an over-stoichiometric heterogeneous catalytic oxidation. The reformate purification is conducted in a subsequent shift stage which enhances the hydrogen concentration. This is followed by an additional selective oxidation step to further refine the hydrogen content. The purification process is carried out in packed-bed reactors.

The reformat is directly distributed to the FCMO which is separated into six modular set up fuel cell systems for easy maintenance and to follow Freudenberg's platform strategy. Each system contains the PEMFC stack as well as balance of plant components such as the compressor, the humidifier as well as the coolant circuit of the stack. The electrical energy produced here is supplied to the ship infrastructure.

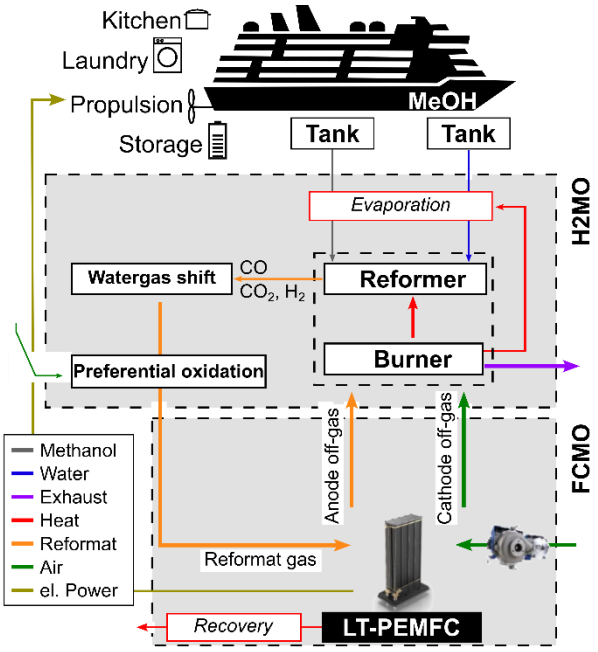

Figure *2* *Setup of a maritime fuel cell system*

2.2 Methanol steam reforming process

According to the system setup the process consists of two main parts – the methanol steam reforming process with its purification process conducted in the H2MO and the electrochemical conversion of hydrogen in the LT PEMFC as a part of the FCMO.

Steam reforming is a common process for hydrogen production for further usage in the chemical industry. The **methanol steam reformation** (MSR) converts methanol and water into CO_2 and H_2 within an endothermic reaction. The steam methanol reforming (Equation (1)), the water gas shift (Equation (2)) and the methanol decomposition (Equation (3)) are the main reactions to describe all reactions running in parallel during the conversion. [39]

$$CH_3OH + H_2O \leftrightarrow CO_2 + 3H_2, \Delta H_0 = 49 \frac{kJ}{mol} \quad (1)$$

$$CO + H_2O \leftrightarrow CO_2 + H_2, \Delta H_0 = -41 \frac{kJ}{mol} \quad (2)$$

$$CH_3OH \leftrightarrow CO + 2H_2, \Delta H_0 = 91 \frac{kJ}{mol} \quad (3)$$

The conversion takes place at a temperature between 200 and 300°C over a CZA (copper/zinc/aluminum) bulk catalyst. Table 2 rates different available catalyst types. Further promotors like ZrO_2 or CeO_2 can be added to enhance the major key characteristics – activity, stability and selectivity – of the catalyst type. [39]

The pressure of the process has a lower influence and normally starts at atmospheric or slightly elevated level.

Table 2 Catalyst rating for MSR (cf. [39–41])

Catalyst type	Cost	Activity	Coking[1]	Thermal stability	Steam stability[2]
Ni	+	+	-	-	+
Cu	+	+	+	-	+
Noble metals (Pt, Pd)	-	++	+	+	++

The MSR process was chosen in contrast to the auto thermal reaction (ATR) as it is less complex which facilitates the controllability of the overall system, cost effectiveness and provides a well-established technology. Further, the start up time is reduced increasing suitability for maritime applications although the ATR is more efficient and produces less CO. [40]

As already mentioned, the purification of the reformat gas is essential. Table 3 summarizes different physical and chemical technologies for purification. **Pressure swing adsorption** (PSA) employs adsorbent materials (e.g., carbon, metal oxides, zeolites, metal-organic frameworks, nanomaterials, or composites) to adhere removable gases to their surfaces under controlled pressure and temperature conditions. This intermittent process requires a low-pressure purging step after each high-pressure adsorption phase. **Membrane separation** (MS) utilizes materials (polymeric, inorganic or mixtures) with specific permeabilities to separate molecules from the flow. **Cryogenic separation** (CS) leverages the differing boiling points of fluid components to separate them by cooling and liquefaction. In the **preferential oxidation** (PROX) process, a highly selective catalyst oxidizes CO in syngas to CO_2, minimizing hydrogen oxidation and methanation.

Table 3 Purification technology rating (cf. [42, 43])

Technology	Purity	Complexity[3]	Energy	Space	Cost
PSA	++	+	+	+	+
MS	+	+	+	++	+
CS	++	-	-	-	-
PROX	+	++	+	+	++
WGS	+	+	+	+	++

The **water gas shift** (WGS) process acts as an enhancer to increase the hydrogen yield while simultaneously decreasing the amount of CO in a slightly exothermic reaction (cf. Equation (2)). Due to its advantageous properties for the methanol steam reforming (MSR) process, the WGS reaction is employed as the initial purification stage for the maritime fuel cell system. When combined with the methanol steam reforming process which operates at temperatures between 200°C and 300°C, a low-temperature water-gas shift reaction is utilized for the MSR which is based on similar catalyst types and shows similar properties. [39]

For the second stage of the purification (cf. [43–46]) the system uses PROX with its simpler integration into the process, its moderate integration volume as well as its cost effectiveness. For the PROX several catalyst types are investigated and under development, including single and bimetallic based catalysts using a single metal from the group platinum (Pt), palladium (Pd), ruthenium (Ru), rhodium (Rh), iridium (IR) or a combination thereof, gold (Au) based single or bimetallic catalyst as well as transitional metal oxide (TMO) catalysts using transitional metals like cerium (Ce), manganese (Mn) or cobalt (Co). Table 4 rates the different catalyst types regarding the risk of methanation, their sensitivity to steam exposure, the selectivity of CO oxidation, the thermal stability and their cost.

Table 4 Catalyst rating for PROX (cf. [45–47])

Catalyst type	Methanation	Selectivity	Therm. stability	Steam sensitivity[4]	Cost
Pt	++	+	+	+	-
Pd	+	+	+	+	+
Ru	-	-	-	-	+
Rh	+	++	+	-	-
Ir	++	+	++	+	-
Bi-metal		++	+		-
Au	++	++	-	+	-
TMO	-	-	-	-	++
Cu	+	+	+	+	++

Depending on the specific catalyst type the exothermic PROX reaction takes place between 80°C and 240°C, both the temperature and the catalyst type having a high impact on the selectivity of the possible reactions. Equation (4) describes the desired CO oxidation whereas Equation (5) describes the unwanted H_2 oxidation. For temperature ranges >200°C and especially for ruthenium (Ru) and partially rhodium (Rh) based catalyst there is an increased risk of methanation described in part by Equation (6) as the CO methanation and by (7) the CO_2 methanation (cf. [45, 47]), which has to be limited because to its high H_2 consumption. Due to Freudenberg's system design the potential risk of methane slip is minimized by feeding the syngas to the burner

[1] Potential of carbon deposit formation on catalyst surface

[2] Refers to how steam content affects the reactivity.

[3] Controllability of purification, integrability into the process.

[4] Refers to how steam affects the CO conversion.

oxidizing the methane before it is expelled to the ambient.

$$CO + \frac{1}{2}O_2 \rightarrow CO_2, \Delta H_0 = -283 \frac{kJ}{mol} \quad (4)$$

$$H_2 + \frac{1}{2}O_2 \rightarrow H_2O, \Delta H_0 = -242 \frac{kJ}{mol} \quad (5)$$

$$CO + 3H_2 \rightarrow CH_4 + H_2O, \Delta H_0 = -206 \frac{kJ}{mol} \quad (6)$$

$$CO_2 + 4H_2 \rightarrow CH_4 + 2H_2O, \Delta H_0 = -165 \frac{kJ}{mol} \quad (7)$$

With steam present in the process platinum and palladium based catalyst promote the CO conversion during the water gas shift reaction of Equation (2), whereas the steam content reduces the CO conversion efficiency for Rh based catalysts (cf. [45]). Using PROX purification requires a precise control of the process conditions at all load points of the maritime fuel cell system. This is essential to prevent the negative effects of high-water content in the stream and to avoid the highly exothermic methanation reaction, which can cause a thermal runaway in the packed bed PROX reactor.

2.3 PEM fuel cell

The FCMO contains the PEMFC system each with its own stack. The stack consists of 346 cells arranged in series. In the stack the electrochemical conversion of the hydrogen rich reformat gas takes place. The hydrogen is provided to the anode side and humidified air is provided to the cathode side of each cell of the stack. There the specific inner assembly of each cell is responsible for the efficiency and functionality of the electrochemical process. The product gases H_2 and air respectively the oxygen content is distributed within the special channel pattern of the **bipolar plates** (BP) over the complete active area of the cathode respectively anode side electrode. The electrodes consist each of:

A gas diffusion layer (GDL) (cf. Figure 3) supporting an enhanced and equal distribution of the product gases over the active area as well as supporting the water management, the heat transfer and guaranteeing the electrical conductance within the layer

A **microporous layer** (MPL) as part of the GDL to enhance the contact to the catalyst layer and its mechanical support as well as to support the water and thermal management

A **catalyst layer** (CL) based on platinum nanoparticles supported on carbon to enable the half reactions on the anode (cf. Equation (9)) and cathode (cf. Equation (8)) side as well as to support the thermal management and the electrical conductivity.

$$\frac{1}{2}O_2 + 2e^- + 2H^+ \rightarrow H_2O \qquad E^0 = 1.23V \quad (8)$$

$$H_2 \rightarrow 2H^+ + 2e^- \qquad E^0 = 0V \quad (9)$$

Each catalyst layer is bonded on the **polymer membrane** (PM). Thus, both electrodes are separated and electrically insulated. The unit is called **membrane electrode assembly** (MEA). The polymer membrane is permeable for protons in humid state which are generated in the anode catalyst by the hydrogen reduction (Equation (9)). With this separation of the reactions the electrochemical potential difference between the two half reactions drives the usable current per cell with 26.8 Ah/mol. The heat generated due to the ohmic losses in the fuel cell is dissipated via the MEA to the cooling channels on the backside of the BP.[34, 48]

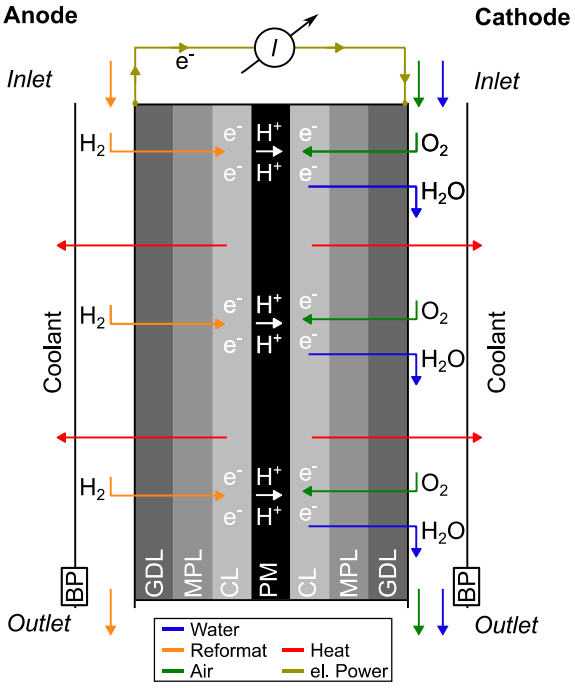

Figure *3* *PEMFC setup*

2.4 Modelling of the system

The coupling of both the methanol steam reforming and the electrochemical conversion of hydrogen requires a detailed knowledge about both processes individually as well as the complex effects of the coupling on the respective other system. Thus, model-based system design is a promising approach to get rid of the complexity and enhance the maturity of the system. For the analysis of the methanol steam reforming process, process simulation tools are employed to evaluate

heat, energy, and species flow under steady-state conditions. These tools help determine the optimal process layout, component sizes and operating conditions. Typically, the analysis focuses on steady-state energy and mass balances, often neglecting detailed component analysis as seen in [14, 43]. For component development, detailed 3D or 2D analyses are necessary, as demonstrated in [49, 50], to derive radially and laterally resolved temperature distributions and conversion efficiencies under varying conditions, such as the steam-to-carbon (SC) ratio. Simplifying these simulations to a one-dimensional approach allows components like reformers (e.g. [51]) to be integrated into complete system simulation models.

Methanol reforming systems are primarily used in stationary chemical applications and rarely undergo transient behavior analysis during startup, shutdown, load changes, or error modes. Load changes are particularly uncommon, as these plants are designed to deliver optimized performance throughout their operational lifetime. However, Tian et al. [52] present a dynamic simulation of a methanol reforming HT-PEMFC system, similar to Freudenberg's maritime fuel cell system, demonstrating its applicability in system design.

Figure 4 summarizes the methodology used to model Freudenberg's maritime fuel cell system within Gamma Technologies 1D- simulation software GT-suite v2025. During the development process the level of detail of the system increased resulting in a more detailed system model including components such as valves, heat exchangers, compressors and reactors within the different fluid circuits specified in the P&ID using component data available from suppliers. Within the final design even detailed piping systems can be specified to enhance the system model's accuracy in pressure drop and flow distribution. During the modelling it is essential to implement an early and reliable verification process so the increasing level of accuracy can already be used in iteration steps to enhance the system quality. Verification data can be derived from literature, more detailed 2D/3D CFD simulations (cf. [34]) or in the best case from component measurement data. It can also be used to calibrate component models or to reduce model complexity to save runtime. The proceeding will be shown using the example of the modelling of the reactor and the fuel cell system.

3 MODELLING OF THE REACTOR

The reactors are the main components in the H2MO realizing the methanol steam reforming process. They are designed as packed bed reactors using appropriate catalysts for each the methanol steam reforming, the shift reaction and the preferential oxidation. To model those components a combination of reaction kinetics, thermal resistance networks and fluid regions is used. To derive the reaction kinetics characterizing lab tests of the used catalysts were performed.

3.1 Methanol steam reformer

The methanol steam reformer is designed as a tubular packed bed reformer using a catalytic combustor as integrated heat generator of the surplus reformat gas not consumed in the fuel cell. The setup follows the arrangement shown in Figure 5 comparable to the findings presented in [51]. To model the phenomena occurring within the reformer tube, the primary conservation equations for energy (cf. Equation 5-1 and 5-2) and mass balance (cf. Equation 5-3 and 5-4) are applied at the inside and the outside of the catalyst tube (cf. Figure 5). The heat transfer of the hot combustion gas flow to the reformer catalyst tube is described by a heat transfer correlation derived from [53] to calculate U_o.

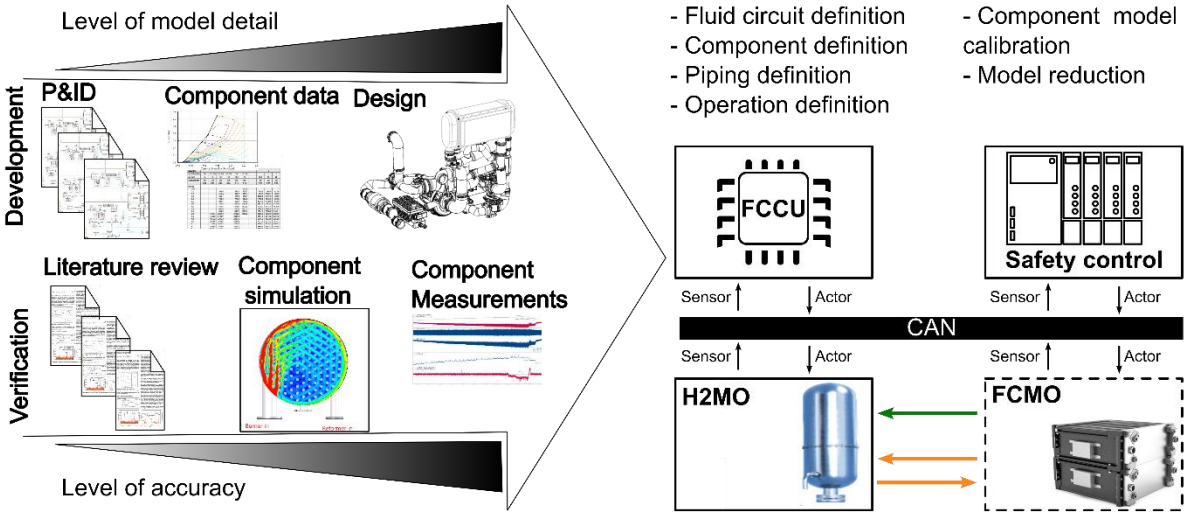

Figure 4 Modelling approach

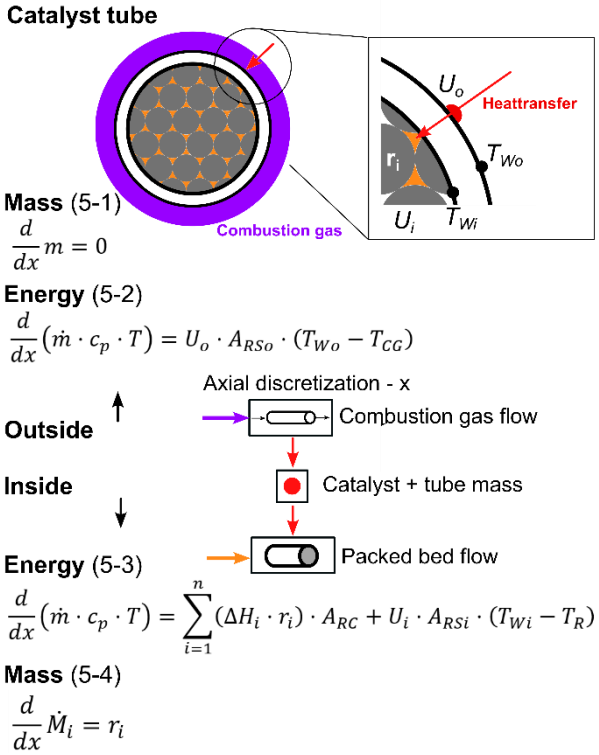

Figure *5* *Heat and mass balance for a catalyst tube*

The heat transfer from the catalyst tube wall to the packed bed is simplified as a simple thermal resistance using the thermal conductivity of the catalyst material but neglecting the convective part from the fluid flow to the tube wall. The heat transfer from the packed bed flow to the catalyst is derived from a Nusselt correlation used for spherical packed beds (cf. [54]) already provided as model template in the software package. Combined with the thermal resistance between the tube wall and the catalyst, the particles U_i can be calculated. To account for the axial temperature distribution the setup is divided into five sections. On the other hand, there is no radial heat distribution which shows a significant impact on the heat transfer and thus on the reaction or respectively the methanol conversion efficiency (cf. [51]). The effect must be compensated with a proper tuning of the heat transfer in the packed bed using appropriate measurement data. The pressure drop in the packed bed is described with the widely used semiempirical Ergun equation (cf. [51]). The reaction rate r_i is calculated with a tuned reaction kinetic thus giving the opportunity to calculate the change of the molar flow rate $\dot{M}_i$for each species and thus the reaction heat $\dot{H}_i$. Two reaction kinetic approaches have been used: a Langmuir-Hinshelwood approach (cf. Equation (10), (11)) as used in [51, 55] and a power law approach (cf. Equation (12), (13)) used e.g. in [56]. Both kinetics take the MSR (Equation (1)) and reverse water gas shift (rWGS) (Equation (*2*)) reaction into account. The measurement results are derived from a lab-scale isothermal packed bed tubular reactor test rig under a variation of inlet temperature from 200-280°C at a fixed inlet flow composition for a commercial Cu/ZnO/Al_2O_3 catalyst.

$$r_{SR} = \frac{k_{SR}\frac{K_{CH_3O(1)}p_{CH_3OH}}{p_{H_2}^{0.5}}\left(1-\frac{p_{H_2}^3 p_{CO_2}}{K_{SR}p_{H_2O}p_{CH_3OH}}\right)}{\left(1+\frac{K_{CH_3O(1)}p_{CH_3OH}}{p_{H_2}^{0.5}}+\frac{K_{OH(1)}p_{H_2O}}{p_{H_2}^{0.5}}+K_{HCOO(1)}p_{H_2}^{0.5}p_{CO_2}\right)\left(1+\sqrt{K_{H(1)}p_{H_2}}\right)} \quad (10)$$

$$r_{rWGS} = \frac{k_{rWGS}K_{HCOO(1)}p_{CO_2}p_{H_2}^{0.5}\left(1-\frac{p_{H_2O}}{K_{rWGS}p_{H_2}p_{CO_2}}\right)}{\left(1+\frac{K_{CH_3O(1)}p_{CH_3OH}}{p_{H_2}^{0.5}}+\frac{K_{OH(1)}p_{H_2O}}{p_{H_2}^{0.5}}+K_{HCOO(1)}p_{H_2}^{0.5}p_{CO_2}\right)^2} \quad (11)$$

$$r_{SR} = k_1 p_{CH_3OH} p_{H_2O} \quad (12)$$

$$r_{rWGS} = k_2 p_{CO_2} p_{H_2} - k_{-2} p_{H_2O} p_{CO} \quad (13)$$

The kinetics are tuned within the software package using a model of the lab-scale isothermal packed bed tubular reactor test rig using the pre-exponent and the activation energy of the Arrhenius approach. Figure 6 shows the comparison of both reaction kinetics compared against five measurement points at different inlet temperatures for the methanol conversion efficiency.

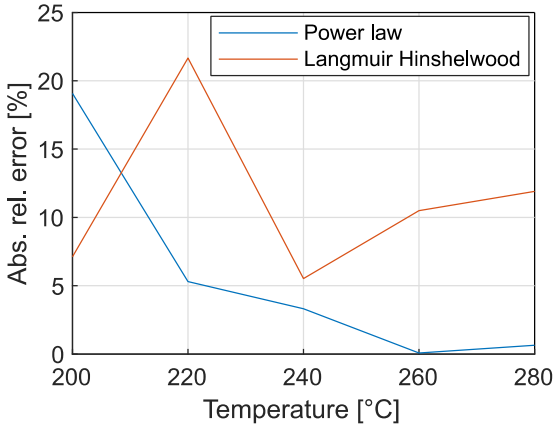

Figure *6* *Comparison-conversion efficiency MEOH*

The Langmuir-Hinshelwood mechanism is normally used to describe heterogeneous reactions on surfaces, considering adsorption-desorption steps and surface reactions. Despite its complexity and challenges with data fitting as seen here, it remains valuable for accurate modeling. In contrast, the power law approach is less complex, expressing reaction rates as functions of reactant concentrations. However, it doesn't account for adsorption and surface reactions, thus being less accurate for heterogeneous catalytic reactions and therefore not commonly used. Nevertheless, the power law approach shows a better fit for the

temperature range of interest at 220-280°C within 5%.

3.2 Preferential oxidation

For the preferential oxidation a packed bed reactor is used. As the reaction is exotherm no additional heat transfer is necessary which simplifies the modelling to the configuration depicted in Figure 7 including a convective heat transfer to the system's internal module space.

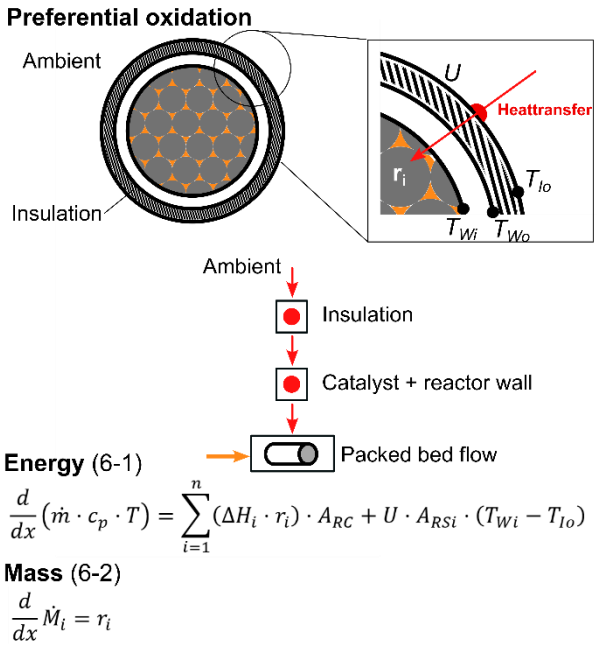

Figure *7* *Heat and mass balance PROX*

The reaction rate r_i for each species is calculated using a reaction kinetic according to the Langmuir Hinshelwood approach comparable to [57]. The used kinetics include the CO oxidation (Equation (4)), hydrogen oxidation (Equation (5)) as well as the CO (Equation (6)) and CO2 ((7)) based methanation reactions. Experimental results for the Ru based catalyst are used to tune the reaction kinetics. Those tests comprise a lab scale isothermal packed bed tubular reactor at fixed inlet composition and space velocity while increasing the temperature up to 200°C. Figure 8 shows the results of the tuned simulation model compared to the experimental data as the absolute value of the relative error calculated according to Equation (14).

$$r = \left| \frac{y_{Measurement} - y_{Simulation}}{y_{Measurement}} \right| \quad (14)$$

The simulation accuracy regarding the transient temperature ramp up is within <5% providing sufficient accuracy to use the kinetics for further investigations about the ramp up behavior of the system.

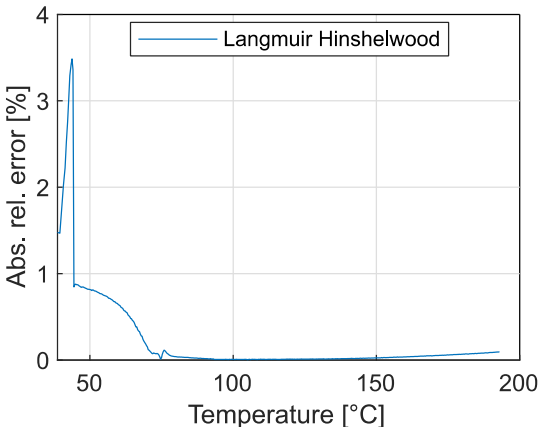

Figure *8* *Comparison-conversion efficiency CO*

3.3 Shift process

For the shift process a packed bed reactor is used showing a similar heat and mass balance as Figure 7. The reaction kinetic is set up as shown in (15) using the partial pressure of the species p_i, the temperature T and the equilibrium constant according to [58].

$$r_{WGS} = k_{WGS}\left(p_{CO}p_{H_2O} - \frac{p_{CO_2}p_{H_2}}{\underbrace{e^{\frac{4577.8}{T} - 4.33}}_{equilibrium\ constant}}\right) \quad (15)$$

With the lack of experimental data to determine accurate kinetics, using this kinetic as a preliminary solution is valid, provided that the process conditions are meticulously controlled to maintain the kinetic balances.

4 MODELLING OF THE PEM FUEL CELL

The PEMFC is analogous to the reactors in the H2MO, the core component of the FCMO. Precise process control is crucial to ensure the efficiency of the PEMFC's electrochemical energy conversion. Therefore, obtaining accurate results from the PEMFC model requires a precise model of the BOP to predict process conditions such as pressure, temperature, and humidity on both the anode and cathode sides, as well as the stack temperature. For the PEMFC, the software package provides a template that integrates the modeling of flow, thermal, electrochemical, and heat domains, simplifying the implementation of the geometry and material data of the stack assembly. The electrochemical correlation is described using the Nernst equation (cf. Equation (16)), which explains the reversible work for a redox reaction under varying temperature and concentration. Due to effects like activation, ohmic and mass transport losses, the Nernst voltage is reduced to the usable voltage.

$$E(T) = E^0 - \frac{R \cdot T}{2 \cdot F} \cdot ln\left(\frac{p_{H_2} \cdot p_{O_2}^{0.5}}{p_{H_2O}}\right) \quad (16)$$

This relationship is described by the cell's polarization curve as a function of the current density, as shown in Figure 9. The polarization curve can be divided into three sections based on current density, with each section contributing significantly to the overall losses (cf. [34]). Each loss is correlated with a semi-empirical formula used in a set of equations to model the fuel cell within the software package.

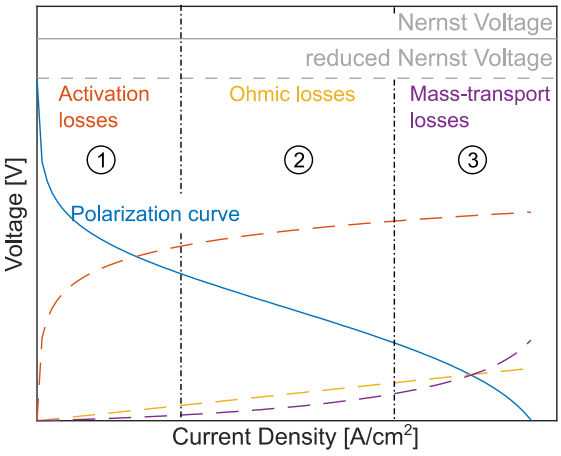

Figure 9 *Polarization curve and losses*

Table 5 summarizes the used correlations. The activation loss considers the reaction kinetics of the two half-cell reactions.

The Tafel equation, a simplified form of the Butler-Volmer equation, incorporates the current density i, the exchange current density i_0, the ideal gas constant R, Farraday's constant F and the charge transfer coefficient α. The exchange current density is calculated using the catalyst specific area A_c, the catalyst loading L_c, the activation energy E and the partial pressure of hydrogen respectively oxygen at the anode respectively the cathode side. The ohmic overpotential is calculated from the membrane thickness t_m experimental coefficients $a - c$ the cell temperature T_c and the membrane water content λ_m. Mass transport losses are primarily caused by the diffusion of reactants through the gas diffusion layer (GDL). At high current densities, this diffusion is hindered by significant water accumulation, resulting in reduced reactant supply and voltage drop. The diffusion is calculated with Fick's law over support nodes within the GDL. The Diffusion coefficient is calculated according to the method shown in [59].

Table 5 Overpotential correlations

Figure 9	Correlation	
1	$\eta_1 = \frac{R \cdot T}{2 \cdot \alpha \cdot F} \cdot ln\left(\frac{i}{i_0}\right)$ $i_0 = i_0^{ref} \cdot A_c \cdot L_c \cdot \frac{p_{A/C}}{p_{ref}} \cdot e^{\frac{E}{R}\left(\frac{1}{T_{ref}} - \frac{1}{T_{cell}}\right)}$	Tafel
2	$\eta_2 = I \cdot \left(\frac{t_{membrane}}{\sigma_{membrane}}\right)$ $\sigma_{membrane} = (a \cdot \lambda_m - b) \cdot e^{c \cdot \left(\frac{1}{303} - \frac{1}{T_{cell}}\right)}$	Springer
3	$J = -D\frac{dC}{dy}$	

The calculated losses are directly converted into heat and added to the coolant flow within the fuel cell using the Colburn heat transfer correlation and a tuned heat transfer multiplier on the coolant side.

The water management within the fuel cell is also an essential part of the model as it determines the membrane's proton conductivity and the gas transport of the reactants within the GDL. For the membrane water content as well as the membrane water diffusivity calculation the Springer equation (cf. [60]) with its empirical coefficients based on membrane humidity and temperature is used.

The model behavior is determined and affected by the tuning of the chosen empirical coefficients used in the mentioned equations. The tuning for the

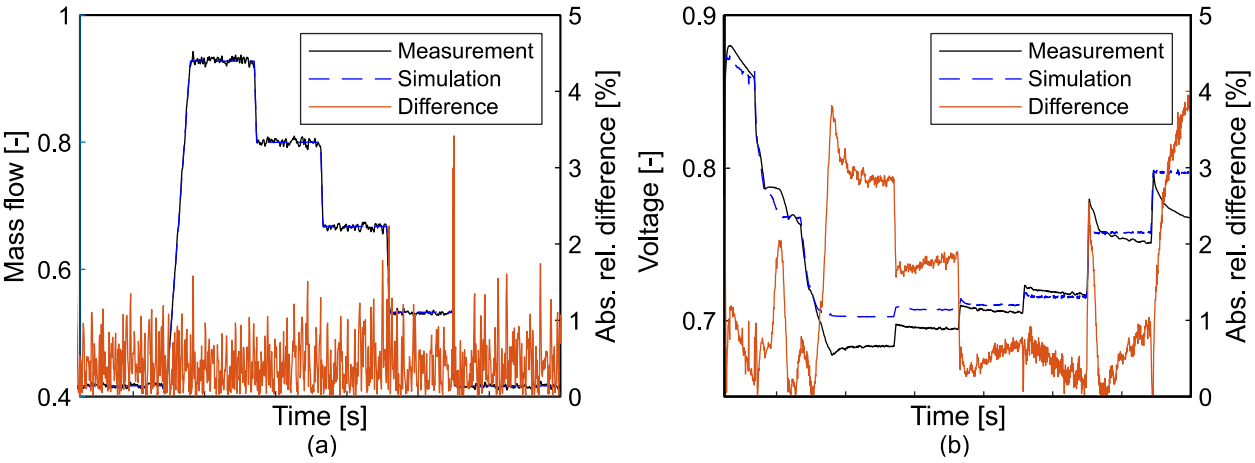

Figure 10 Evaluation FC Model - (a) Cathode mass flow (b) Stack voltage

model and its accuracy regarding the fuel cell is described in [34]. The tuning was carried out using single cell measurements using a fixed reformat composition resulting in a deviation of less than 3%. In a full system simulation context, a proper tuning of components is essential to gain a high model accuracy.

An initial comparison of the fuel cell system model to testing data, including the PEMFC stack and the balance of plant components, demonstrates the model's accuracy. Figure 10 presents the measurement and simulation data during a test run for (a) the cathode mass flow and (b) the stack voltage each scaled to the maximum value. These tests were conducted at Freudenberg's internal testing rigs using pure hydrogen instead of syngas. The measurement data was processed using a Gaussian filter to minimize measurement noise. The absolute value of the relative error was calculated according to Equation (14). The model's accuracy for both values shown is within 5% for the entire range of operation. The cathode mass flow behavior (cf. Figure 10 (a)) is primarily determined by the compressor, which is modeled with a compressor map based on supplier data and the precise mapping of the flow path, including all pressure losses of the installed components. The transient behavior of the mass flow during load changes, which is crucial for accurately predicting control responses, is well-represented. Comparing the mean absolute value of the relative difference for stack voltage (1.5%) and cathode mass flow (0.8%), it becomes evident that deviations in the simulation concerning stack temperature and stack tuning accuracy contribute to the overall model discrepancies. As the anode mass flow is provided with an appropriate controlled boundary condition it is not contributing here. Nevertheless, with a relative difference of less than 5%, the model demonstrates sufficient accuracy to be used for further investigations.

5 SYSTEM SIMULATION

The system simulation of Freudenberg's maritime fuel cell system uses the setup shown in Figure 4. The control and safety functions required to operate the system are implemented within the GT-model environment as well, which facilitates the further development of these functions. Depending on the scope of the investigation, the model can be simplified; for instance, the FCMO module is neglected during the startup phase of the H2MO system. However, during the load run of the system, both the FCMO and H2MO modules are utilized. The system simulation is configured to run using GT's implicit solver, which ensures faster runtimes. Dependant on the systems operation state the time step is adjusted automatically ensuring the best compromise between runtime and convergence. chemistry solver designed to handle differential-algebraic equations (DAEs). To accurately solve the chemical reactions, the software package includes a Specifically, a DASSL solver is employed to manage the stiff kinetics present in the system. The rWGS reaction in the MSR exhibits a particularly fast reaction rate. This rapid rate significantly contributes to the system's stiffness, especially during startup conditions when the concentrations of reactants change quickly until a stable and steady operation is achieved.

Figure 11 shows the hydrogen generation during the system run up. Between the start of media supply and the first hydrogen peak it takes six minutes to fill the piping system and heat exchangers with the fluids and start the evaporation process. To reduce carbon decomposition of the reformer catalyst, water vapor is introduced first to avoid exposing the catalyst to pure methanol. Additionally, the higher heat capacity of water vapor reduces the risk of hot spot formation within the catalyst. Once methanol vapor is provided, hydrogen generation begins and stabilizes after 15 minutes. In total, around 21 minutes are necessary from the supply of the fluids to achieve stabilized hydrogen production after starting with a preheated system.

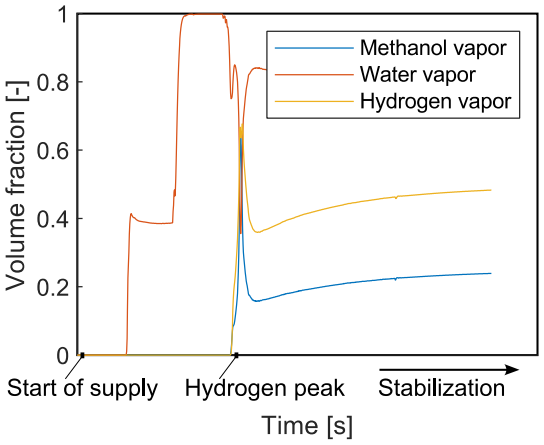

Figure 11 Hydrogen generation during start up

The system model is used beside the insight into the transient start up process to tune the control loops of the system. Figure 12 shows the methanol control valve over a ramp up of the system power from idle to full load. For a better visibility the left and right half of the curve are depicted over different scaling of the y-axis. The deviation is derived according to Equation (14) showing high deviation in the beginning of the control due to a delay in the control of 0.5s including the CAN communication and the valve opening and closing times. Nevertheless, the control shows no overshoot and the deviation diminishes over time.

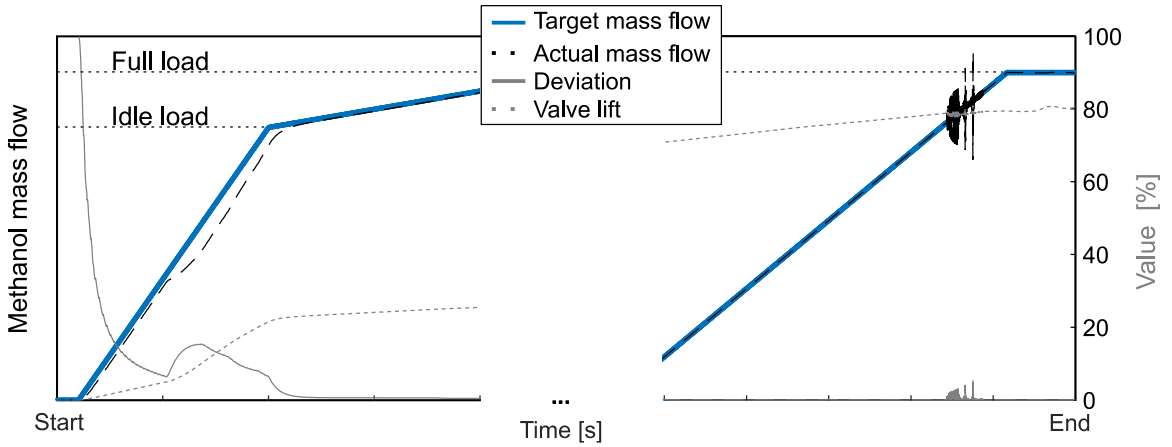

Figure 12 Methanol flow control during system power ramp up

6 CONCLUSIONS

The paper shows Freudenberg's maritime fuel cell system realizing a methanol steam reforming process to provide a H_2 rich reformat gas to a LT PEMFC. The presented modelling of the key components of both processes shows a high accuracy of the 1D-System simulation compared with preliminary component measurements.

However, the lack of resolution perpendicular to the flow in the 1D simulation approach results in an overpredicted temperature of the packed beds, particularly during startup and load changes. This issue can be mitigated by adjusting the heat transfer coefficients within the packed beds and the reformer. Initial comparisons of heat transfer with CFD results indicate deviations within a 5% range of the 1D approach.

The comparison of the Langmuir-Hinshelwood with the power law approach for the MSR showed that an insufficient set of data to tune the high number of parameters leads to a misleading prediction of the conversion efficiency with high deviations for the Langmuir Hinshelwood approach. With the power law the deviation in the useful temperature range is less than 5% as well.

On the other hand, the tuning of the Langmuir Hinshelwood approach shows a good accuracy for the PROX kinetics due to sufficient experimental data also with an absolute value of the relative error less than 5% over the measured temperature ramp.

The PEMFC model shows a good correspondence between simulation and measurement data, for steady operation as well as for transient load changes already within a deviation of less than 4%.

The verified models are used to predict the transient system behavior during start up predicting the time until the first hydrogen generation and tune the control loop functions.

Further measurement taken from the complete system will be used to validate the accuracy of the complete system simulation as well as provide the opportunity to improve the model accuracy to be used for further system optimization and development.

7 ABBREVIATIONS

ATR	Autothermal reaction
BP	Bipolar plate
CL	Catalyst layer
CS	Cryogenic separation
CZA	Copper zink aluminum
ECA	Emission controlled area
ETS	European trading system
FCMO	Fuel cell module
GDL	Gas diffusion layer
GHG	Green house gas emissions
H2MO	Hydrogen module
HCCI	Homogeneous charge compression ignition
HT	High temperature
IMO	International maritime organization
LT	Low temperature
MCFC	Molten carbonate fuel cell
MDO	Marine Diesel Oil
MEA	Membrane electrode assembly
MPL	Microporous layer
MS	Membrane separation
MSR	Methanol steam reforming
PEMFC	Proton exchange membrane fuel cell
PM	Polymer membrane
PROX	Preferential oxidation
PSA	Pressure swing adsorption
RCCI	Reactivity controlled compression ignition
rWGS	Reverse water gas shift
SC	Steam to carbon
SOFC	Solid oxide fuel cell
WGS	Water gas shift

8 ACKNOWLEDGMENTS

The authors would like to thank Christian Altenhofen from Gamma Technology for the good collaboration and support. Further we have to mention the support of Brijesh Goyani and Saumya Ghandi from Freudenberg e-Power Systems contributing to realize the results.

9 REFERENCES

[1] UNCTAD, *Review of maritime transport 2023: Towards a green and just transistion.* [Online]. Available: https://digitallibrary.un.org (accessed: Dec. 28 2024).

[2] A. I. Osman, M. Nasr, E. Lichtfouse, M. Farghali, and D. W. Rooney, "Hydrogen, ammonia and methanol for marine transportation," *Environ Chem Lett*, vol. 22, no. 5, pp. 2151–2158, 2024, doi: 10.1007/s10311-024-01757-9.

[3] A. Nazemian, E. Boulougouris, and S. K. Melemadom, "Hybrid and Alternative Fuel Power Management Systems in Ships – Multi-Criteria Decision-Making Assessment," in.

[4] DNV-GL, *Comparison of Alternative Marine Fuels.* [Online]. Available: https:// safety4sea.com (accessed: Dec. 28 2024).

[5] Y.-H. Pu, Q. Dejaegere, M. Svensson, and S. Verhelst, "Renewable Methanol as a Fuel for Heavy-Duty Engines: A Review of Technologies Enabling Single-Fuel Solutions," *Energies*, vol. 17, no. 7, p. 1719, 2024, doi: 10.3390/en17071719.

[6] Lindgren, M., Schröder, J., Winther, K., Müller-Langer, F., Baumgarten, W., & Aakko-Saksa, P., *Methanol as a Marine Fuel: Environmental Benefits, Technology Readiness, and Economic Feasibility.* [Online]. Available: https://www.iea-amf.org

[7] Methanol Institute, *Renewable Methanol.* [Online]. Available: https://www.methanol.org (accessed: Dec. 29 2024).

[8] M. Alnajideen *et al.,* "Ammonia combustion and emissions in practical applications: a review," *Carb Neutrality*, vol. 3, no. 1, 2024, doi: 10.1007/s43979-024-00088-6.

[9] S. Mashruk *et al.,* "Perspectives on NO X Emissions and Impacts from Ammonia Combustion Processes," *Energy & fuels : an American Chemical Society journal*, vol. 38, no. 20, pp. 19253–19292, 2024, doi: 10.1021/acs.energyfuels.4c03381.

[10] Q. Cheng, A. Muhammad, O. Kaario, Z. Ahmad, and L. Martti, "Ammonia as a sustainable fuel: Review and novel strategies," *Renewable and Sustainable Energy Reviews*, vol. 207, p. 114995, 2025, doi: 10.1016/j.rser.2024.114995.

[11] R. Novella, J. Pastor, J. Gomez-Soriano, and J. S. Bayona, "Challenges and Directions of Using Ammonia as an Alternative Fuel for Internal Combustion Engines," doi: 10.4271/2023-01-0324.

[12] V. J. Reddy, N. P. Hariram, R. Maity, M. F. Ghazali, and S. Kumarasamy, "Sustainable E-Fuels: Green Hydrogen, Methanol and Ammonia for Carbon-Neutral Transportation," *WEVJ*, vol. 14, no. 12, p. 349, 2023, doi: 10.3390/wevj14120349.

[13] G. Finger and G. Prause, "On Safety Aspects of Ammonia as Marine Fuel," in pp. 57–65.

[14] J. Zhang, Z. Zhang, and D. Liu, "Comparative Study of Different Alternative Fuel Options for Shipowners Based on Carbon Intensity Index Model Under the Background of Green Shipping Development," *JMSE*, vol. 12, no. 11, p. 2044, 2024, doi: 10.3390/jmse12112044.

[15] N. Kawahara and U. Azimov, "Abnormal Combustion in Hydrogen-Fuelled IC Engines," pp. 459–482, doi: 10.1007/978-3-031-28412-0_12.

[16] P. Grabner, M. Schneider, and K. Gschiel, "Formation Mechanisms and Characterization of abnormal Combustion Phenomena of Hydrogen Engines," doi: 10.4271/2023-32-0168.

[17] A. Franco and C. Giovannini, "Hydrogen Gas Compression for Efficient Storage: Balancing Energy and Increasing Density," *Hydrogen*, vol. 5, no. 2, pp. 293–311, 2024, doi: 10.3390/hydrogen5020017.

[18] S. O. Rey *et al.,* "Powering the Future: A Comprehensive Review of Battery Energy Storage Systems," *Energies*, vol. 16, no. 17, p. 6344, 2023, doi: 10.3390/en16176344.

[19] Mærsk Mc-Kinney Møller Center for Zero Carbon Shipping, *Fuel Cell Technologies and Applications for Deep-Sea Shipping.* [Online]. Available: https:// www.zerocarbonshipping.com (accessed: Dec. 29 2024).

[20] MaritimeCyprus, *Maritime Innovation Report.* [Online]. Available: ttps:// www.maritimecyprus.com/ (accessed: Dec. 29 2024).

[21] H. Xing, C. Stuart, S. Spence, and H. Chen, "Fuel Cell Power Systems for Maritime Applications: Progress and Perspectives,"

Sustainability, vol. 13, no. 3, p. 1213, 2021, doi: 10.3390/su13031213.

[22] L. van Biert, M. Godjevac, K. Visser, and P. V. Aravind, "A review of fuel cell systems for maritime applications," *Journal of Power Sources*, vol. 327, pp. 345–364, 2016, doi: 10.1016/j.jpowsour.2016.07.007.

[23] Tomas Tronstad, Hanne Høgmoen Åstrand, Gerd Petra Haugom, and Lars Langfeldt, "Maritime Study on the use of Fuel Cells in Shipping,"

[24] S. Mo *et al.,* "Recent Advances on PEM Fuel Cells: From Key Materials to Membrane Electrode Assembly," *Electrochem. Energy Rev.*, vol. 6, no. 1, 2023, doi: 10.1007/s41918-023-00190-w.

[25] N. Laosiripojana, W. Wiyaratn, W. Kiatkittipong, A. Arpornwichanop, A. Soottitantawat, and S. Assabumrungrat, "Reviews on Solid Oxide Fuel Cell Technology," *EJ*, vol. 13, no. 1, pp. 65–84, 2009, doi: 10.4186/ej.2009.13.1.65.

[26] L. van Biert, M. Godjevac, K. Visser, and P. V. Aravind, "A review of fuel cell systems for maritime applications," *Journal of Power Sources*, vol. 327, pp. 345–364, 2016, doi: 10.1016/j.jpowsour.2016.07.007.

[27] B. Wu, M. Matian, and G. J. Offer, "Hydrogen PEMFC system for automotive applications," *International Journal of Low-Carbon Technologies*, vol. 7, no. 1, pp. 28–37, 2012, doi: 10.1093/ijlct/ctr026.

[28] G. Schuh, L. Schenk, and P. Scholz, "Use Cases for Fuel Cells in the Commercial Vehicle Sector," *MTZ Worldw*, vol. 83, 2-3, pp. 16–23, 2022, doi: 10.1007/s38313-021-0760-x.

[29] C. Dall'Armi, D. Pivetta, and R. Taccani, "Hybrid PEM Fuel Cell Power Plants Fuelled by Hydrogen for Improving Sustainability in Shipping: State of the Art and Review on Active Projects," *Energies*, vol. 16, no. 4, p. 2022, 2023, doi: 10.3390/en16042022.

[30] S. Krummrich, "Fuel Cell Methanol Reformer System for Submarines," in *Schriften des Forschungszentrums Jülich Reihe Energie & Umwelt*, Bd. 78,3, *18th World Hydrogen Energy Conference 2010 - WHEC 2010: Proceedings*, D. Stolten and T. Grube, Eds., Jülich: Forschungszentrum IEF-3, 2010.

[31] DNV-GL, "Handbook for hydrogen-fuelled vessels," MarHySafe 1st Edition, Jun. 2021.

[32] American Bureau of Shipping (ABS), *Fuel Cell Power Systems for Marine and Offshore Applications.* [Online]. Available: https://ww2.eagle.org

[33] E. B. Agyekum, J. D. Ampah, T. Wilberforce, S. Afrane, and C. Nutakor, "Research Progress, Trends, and Current State of Development on PEMFC-New Insights from a Bibliometric Analysis and Characteristics of Two Decades of Research Output," *Membranes*, vol. 12, no. 11, 2022, doi: 10.3390/membranes12111103.

[34] V. Damerow, K. Chotaliya, S. Karmann, and M. Stefener, "Simulation-based Development of Maritime PEM Fuel Cell Systems," *MTZ Worldw*, vol. 85, no. 5, pp. 40–45, 2024, doi: 10.1007/s38313-024-1911-7.

[35] A. G. Elkafas, M. Rivarolo, E. Gadducci, L. Magistri, and A. F. Massardo, "Fuel Cell Systems for Maritime: A Review of Research Development, Commercial Products, Applications, and Perspectives," *Processes*, vol. 11, no. 1, p. 97, 2023, doi: 10.3390/pr11010097.

[36] Danilo Russo*, Martina De Martino, Almerinda Di Benedetto, Maria Portarapillo, "Oxidative Methanol Reforming for Hydrogen-fed HT-PEMFC: Applications in the Naval Sector," *Journal of Maritime Technology*, vol.15, no. 3, pp. 123–145, 2023, doi: 10.3303/CET2399062.

[37] H. Lee, I. Jung, G. Roh, Y. Na, and H. Kang, "Comparative Analysis of On-Board Methane and Methanol Reforming Systems Combined with HT-PEM Fuel Cell and CO2 Capture/Liquefaction System for Hydrogen Fueled Ship Application," *Energies*, vol. 13, no. 1, p. 224, 2020, doi: 10.3390/en13010224.

[38] O. A. Petrii, "Pt–Ru electrocatalysts for fuel cells: a representative review," *J Solid State Electrochem*, vol. 12, no. 5, pp. 609–642, 2008, doi: 10.1007/s10008-007-0500-4.

[39] M. Zhang *et al.,* "Recent Advances in Methanol Steam Reforming Catalysts for Hydrogen Production," *Catalysts*, vol. 15, no. 1, p. 36, 2025, doi: 10.3390/catal15010036.

[40] M. Rostami, A. H. Farajollahi, R. Amirkhani, and M. E. Farshchi, "A review study on methanol steam reforming catalysts: Evaluation of the catalytic performance, characterizations, and operational parameters," *AIP Advances*, vol. 13, no. 3, p. 30701, 2023, doi: 10.1063/5.0137706.

[41] S. Sá, H. Silva, L. Brandão, J. M. Sousa, and A. Mendes, "Catalysts for methanol steam reforming—A review," *Applied Catalysis B:*

Environmental, vol. 99, 1-2, pp. 43–57, 2010, doi: 10.1016/j.apcatb.2010.06.015.

[42] Naquash, A., Qyyum, M. A., Chaniago, Y. D., Riaz, A., Sial, N. R., Islam, M., Min, S., Lim, H., & Lee, M., Ed., *Membrane-and-Cryogenic-Assisted Hydrogen Separation and Purification Process*, 2021.

[43] A. Graeeli, M. Rahimi-Esbo, V. Kord Firouzjaee, M. Sedighi, and M. Rezaee Firouzjaee, "Steam Reforming of Methanol and Reactor Optimization for Additional Hydrogen Production: Process Simulation," *IJEE*, vol. 15, no. 2, pp. 142–150, 2024, doi: 10.5829/ijee.2024.15.02.03.

[44] M. Ouzounidou, D. Ipsakis, S. Voutetakis, S. Papadopoulou, and P. Seferlis, "A combined methanol autothermal steam reforming and PEM fuel cell pilot plant unit: Experimental and simulation studies," *Energy*, vol. 34, no. 10, pp. 1733–1743, 2009, doi: 10.1016/j.energy.2009.06.031.

[45] T.-S. Nguyen, F. Morfin, M. Aouine, F. Bosselet, J.-L. Rousset, and L. Piccolo, "Trends in the CO oxidation and PROX performances of the platinum-group metals supported on ceria," *Catalysis Today*, vol. 253, pp. 106–114, 2015, doi: 10.1016/j.cattod.2014.12.038.

[46] H. Liu *et al.,* "Recent advances on catalysts for preferential oxidation of CO," *Nano Res.*, vol. 16, no. 4, pp. 4399–4410, 2023, doi: 10.1007/s12274-022-5182-9.

[47] F. Mariño, C. Descorme, and D. Duprez, "Supported base metal catalysts for the preferential oxidation of carbon monoxide in the presence of excess hydrogen (PROX)," *Applied Catalysis B: Environmental*, vol. 58, 3-4, pp. 175–183, 2005, doi: 10.1016/j.apcatb.2004.12.008.

[48] P. Kurzweil, *Brennstoffzellentechnik*. Wiesbaden: Springer Fachmedien Wiesbaden, 2016.

[49] Y. Hu, C. Han, W. Li, Q. Hu, H. Wu, and Q. Li, "Numerical Analysis of Methanol Steam Reforming Reactor for kW-Scale Fuel Cells," vol. 394, pp. 11–20, doi: 10.1007/978-981-99-8585-2_2.

[50] V. Gurau, A. Ogunleke, and F. Strickland, "Design of a methanol reformer for on-board production of hydrogen as fuel for a 3 kW High-Temperature Proton Exchange Membrane Fuel Cell power system," *International Journal of Hydrogen Energy*, vol. 45, no. 56, pp. 31745–31759, 2020, doi: 10.1016/j.ijhydene.2020.08.179.

[51] J. Zhu, S. S. Araya, X. Cui, S. L. Sahlin, and S. K. Kær, "Modeling and Design of a Multi-Tubular Packed-Bed Reactor for Methanol Steam Reforming over a Cu/ZnO/Al2O3 Catalyst," *Energies*, vol. 13, no. 3, p. 610, 2020, doi: 10.3390/en13030610.

[52] *Proceedings of the Asian Modelica Conference*.

[53] P. Stephan, S. Kabelac, M. Kind, D. Mewes, K. Schaber, and T. Wetzel, *VDI-Wärmeatlas*. Berlin, Heidelberg: Springer Berlin Heidelberg, 2019.

[54] R. B. Bird, W. E. Stewart, and E. N. Lightfoot, *Transport phenomena*. New York, Chichester, Weinheim, Brisbane, Singapore, Toronto: John Wiley & Sons Inc, 2007.

[55] S. Sá, J. M. Sousa, and A. Mendes, "Steam reforming of methanol over a CuO/ZnO/Al2O3 catalyst, part I: Kinetic modelling," *Chemical Engineering Science*, vol. 66, no. 20, pp. 4913–4921, 2011, doi: 10.1016/j.ces.2011.06.063.

[56] H. Purnama, T. Ressler, R. Jentoft, H. Soerijanto, R. Schlögl, and R. Schomäcker, "CO formation/selectivity for steam reforming of methanol with a commercial CuO/ZnO/Al2O3 catalyst," *Applied Catalysis A: General*, vol. 259, no. 1, pp. 83–94, 2004, doi: 10.1016/j.apcata.2003.09.013.

[57] P. Garbis, C. Kern, and A. Jess, "Kinetics and Reactor Design Aspects of Selective Methanation of CO over a Ru/γ-Al2O3 Catalyst in CO2/H2 Rich Gases," *Energies*, vol. 12, no. 3, p. 469, 2019, doi: 10.3390/en12030469.

[58] J.M. Moe, "Design of water-gas shift reactors," *Chem. Eng. Prog*, Vol. 58:3, 1962.

[59] E. N. Fuller, P. D. Schettler, and J. C. Giddings, "NEW METHOD FOR PREDICTION OF BINARY GAS-PHASE DIFFUSION COEFFICIENTS," *Industrial & Engineering Chemistry*, vol. 58, no. 5, pp. 18–27, 1966, doi: 10.1021/ie50677a007.

[60] T. Springer, T. Zawodzinski, and S. Gottesfeld, "Polymer Electrolyte Fuel Cell model," *Journal o. Electrochem. Soc.*, no. 138, 1991.

10 CONTACT

Dr.-Ing. Stephan Karmann,Teamlead for Model-Based System Design
Freudenberg Fuel Cell e-Power Systems GmbH
Bayerwaldstraße 3, 81737 Munich
Stephan.Karmann@freudenberg-eps.com